

Thin, soft, skin-integrated electronics for real-time and wireless detection of uric acid in sweat

Yue Hu, Lan Wang, Jian Li, Yawen Yang, Guangyao Zhao, Yiming Liu, Xingcan Huang, Pengcheng Wu, Binbin Zhang, Yanli Jiao, Mengge Wu, Shengxin Jia, Qiang Zhang, Guoqiang Xu, Rui Shi, Dengfeng Li, Yingchun Li, Zhengchun Peng & Xinge Yu

To cite this article: Yue Hu, Lan Wang, Jian Li, Yawen Yang, Guangyao Zhao, Yiming Liu, Xingcan Huang, Pengcheng Wu, Binbin Zhang, Yanli Jiao, Mengge Wu, Shengxin Jia, Qiang Zhang, Guoqiang Xu, Rui Shi, Dengfeng Li, Yingchun Li, Zhengchun Peng & Xinge Yu (24 Jul 2023): Thin, soft, skin-integrated electronics for real-time and wireless detection of uric acid in sweat, International Journal of Smart and Nano Materials, DOI: [10.1080/19475411.2023.2236997](https://doi.org/10.1080/19475411.2023.2236997)

To link to this article: <https://doi.org/10.1080/19475411.2023.2236997>



© 2023 The Author(s). Published by Informa UK Limited, trading as Taylor & Francis Group.



[View supplementary material](#)



Published online: 24 Jul 2023.



[Submit your article to this journal](#)



Article views: 776



[View related articles](#)



[View Crossmark data](#)

Thin, soft, skin-integrated electronics for real-time and wireless detection of uric acid in sweat

Yue Hu^{a,b}, Lan Wang^c, Jian Li^{a,d}, Yawen Yang^a, Guangyao Zhao^a, Yiming Liu^a, Xingcan Huang^a, Pengcheng Wu^a, Binbin Zhang^{a,d}, Yanli Jiao^a, Mengge Wu^a, Shengxin Jia^{a,d}, Qiang Zhang^a, Guoqiang Xu^a, Rui Shi^a, Dengfeng Li^a, Yingchun Li^e, Zhengchun Peng^b and Xinge Yu^{a,d,f}

^aDepartment of Biomedical Engineering, City University of Hong Kong, Hong Kong, P.R. China; ^bState Key Laboratory of Radio Frequency Heterogeneous Integration (Shenzhen University), College of Physics and Optoelectronic Engineering, Shenzhen University, Shenzhen, P. R. China; ^cTransfusion Department, Sichuan Provincial People's Hospital, University of Electronic Science and Technology of China, Chengdu, P.R. China; ^dHong Kong Center for Cerebra-Cardiovascular Health Engineering, Hong Kong Science Park, New Territories, Hong Kong, P.R. China; ^eCollege of Science, Harbin Institute of Technology (Shenzhen), Shenzhen, Guangdong, P. R. China; ^fCAS-CityU Joint Laboratory for Robotic Research, Shenzhen Research Institute City University of Hong Kong, Shenzhen, P.R. China

ABSTRACT


Wearable sweat sensors are gaining significant attention due to their unparalleled potential for noninvasive health monitoring. Sweat, as a kind of body fluid, contains informative physiological indicators that are related to personalized health status. Advances in wearable sweat sampling and routing technologies, flexible, and stretchable materials, and wireless digital technologies have led to the development of integrated sweat sensors that are comfortable, flexible, light, and intelligent. Herein, we report a flexible and integrated wearable device via incorporating a microfluidic system and a sensing chip with skin-integrated electronic format toward in-situ monitoring of uric acid (UA) in sweat that associates with gout, cardiovascular, and renal diseases. The microfluidic system validly realizes the real-time capture perspiration from human skin. The obtained detection range is 5–200 μM and the detection limit is 1.79 μM , which offers an importance diagnostic method for clinical relevant lab test. The soft and flexible features of the constructed device allows it to be mounted onto nearly anywhere on the body. We tested the sweat UA in diverse subjects and various body locations during exercise, and similar trends were also observed by using a commercial UA assay kit.


ARTICLE HISTORY

Received 26 April 2023
Accepted 11 July 2023

KEYWORDS

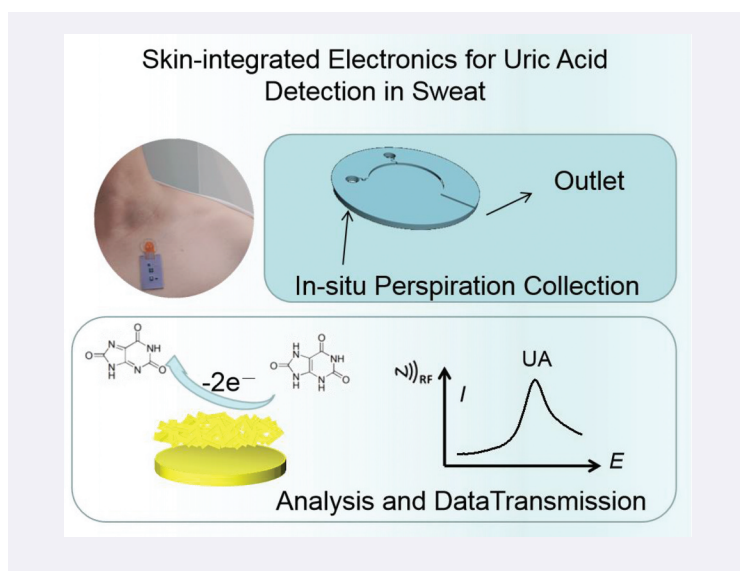
Sweat sensors; skin-integrated electronics; in-situ detection; microchannels; wearable device

CONTACT Zhengchun Peng  zcpeng@szu.edu.cn  State Key Laboratory of Radio Frequency Heterogeneous Integration (Shenzhen University), College of Physics and Optoelectronic Engineering, Shenzhen University, Shenzhen 518060, P. R. China; Xinge Yu  xingeyu@cityu.edu.hk  Department of Biomedical Engineering, City University of Hong Kong, Hong Kong 999077, P.R. China

 Supplemental data for this article can be accessed online at <https://doi.org/10.1080/19475411.2023.2236997>

© 2023 The Author(s). Published by Informa UK Limited, trading as Taylor & Francis Group.

This is an Open Access article distributed under the terms of the Creative Commons Attribution License (<http://creativecommons.org/licenses/by/4.0/>), which permits unrestricted use, distribution, and reproduction in any medium, provided the original work is properly cited. The terms on which this article has been published allow the posting of the Accepted Manuscript in a repository by the author(s) or with their consent.



Introduction

With the rapidly growing demand for digital healthy monitoring, increasing interest in miniaturized and integrated diagnostic devices have been driven [1,2]. Wearable devices integrated with sensors and electronics in particular have the advantages of non-invasively and quickly capturing changes in healthy indicators [3–5]. Recent studies revealed that sweat is an important body fluid for healthy management, disease diagnosis, and sports performance evaluation [6–10]. For example, excessive levels of Ca^{2+} in sweat results in cirrhosis, renal failure, and acid-base balance disorders [11–13]. The concentration of lactic acid in sweat is the gold standard to diagnose lactic acidosis, tissue hypoxia, and respiratory [14,15]. Furthermore, sweat remains relatively easy to access due to the fact that sweat glands are distributed throughout the entire surface of the body unlike other biofluids (such as saliva, interstitial fluid, and urine) [16]. In addition to sweating through physical exertion which is the most common way of sweat sampling [17,18], many other techniques have been proposed for non-invasively extracting sweat till date, including thermal stimulation [19], chemical stimulation [20], or ion osmosis [21]. To sum up, it is meaningful and achievable to develop convenient and reliable wearable devices to offer insight into healthy status by analyzing the dynamics of the concentration of targets in sweat. To date, most of the current development of wearable sensors focused on electrolytes (Na^+ , K^+ , and Cl^-) or metabolites such as glucose and lactic acid, which are made possible by ion-selective or enzyme-modified electrodes, respectively.

UA is the ultimate metabolite of purine metabolism, which has been proved and adopted as a vital indicator for the diagnosis of gout [22–25]. According to relevant literature reports, the concentration of UA in sweat has a certain correlation with blood [26,27]. Thus, tracking the concentration of UA in sweat during daily life is beneficial for reducing risk of gout. UA has also been widely used as a biomarker for cardiovascular [28,29], renal diseases [30], and type 2 diabetes [31,32]. Nevertheless,

the development of a reliable and integrated wearable device for UA monitoring in human sweat remains a challenge as the result of difficulties in its low concentration, the design of sweat sampling system, and the integration of flexible and wearable sweat device. At present, compared with capillary electrophoresis [33], high-performance liquid chromatography [34], and fluorescence spectroscopy [35] which require bulky instruments and complex operating procedures, electrochemical sensors are extremely suitable for wearable sweat devices due to their rapid response, high sensitivity, and simple construction [36,37].

In this work, we report a flexible and wearable sweat monitoring device which integrates with a UA biosensing system and a polydimethylsiloxane (PDMS)-based microfluidic system. It enables in-situ perspiration collection and analysis, as well as wireless data transmission. In detail, the sweat excreted by epidermis can be gathered spontaneously through the inlet microchannels to the target detection chamber. Meanwhile, the outlet microchannel ensures fresh sweat collection and analysis. For the UA sensing chamber, a three-electrode electrochemical sensor modified with nano Au is adopted based on Au electrodes. The resulted UA sensor exhibit great sensing linearity between current responses at the specific potential and the targeted UA concentrations. Furthermore, by virtue of integration with a flexible circuit board and a soft encapsulation layer, the system can be mounted onto skin comfortably and fulfill wireless and real-time detection, demonstrating great potential in daily healthcare.

Results and discussion

Epidermal flexible device for sweat sensing

The skin-integrated sweat collection and monitoring device contains a UA sensor unit based on PI substrate, a microfluidic system based on PDMS substrate, and a medical adhesive layer as exhibited in [Figure 1a](#), where the key components were manufactured using simple and mature photolithography and 3D printed techniques. As these parts are both constructed on the ultra-thin and soft substrates, the final integrated device was flexible ([Figure S1](#) and [S2](#)) and can be bent and twisted serving for body motions. In [Figure 1b](#), the diameter of each electrode in the three-electrode system was set to 3 mm. After individual modification, nano Au, Ag/AgCl, and Au electrodes were used as working, reference, and counter electrodes, respectively ([Figure 1c](#)). The design sketch of the fabricated microfluidic system is illustrated in [Figure 1d](#). The constructed system could non-invasively gather and routing sweat UA. For further realizing miniaturization and integration, the above sensing patch was connected to a flexible printed circuit board (FPCB) as displayed in [Figure 1f](#). The corresponding system-level block diagram in [Figure 1g](#) describes the flow of electrical signals in the electrochemical measurements. The circuit mainly consists of a Microcontroller (MCU), a embedded Analog-to-Digital Converter (12-bits ADC), a Digital-to-Analog Converter (16-bits DAC), a Dual Operational Amplifier (Dual OP-AMP), and an NFC chip. The NFC chip along with energy-harvesting capacities out of the RF field powers external devices. The electronics consuming of our sensing device is 14.4 mW. The Dual OP-AMP is applied to compose the three-electrode system.

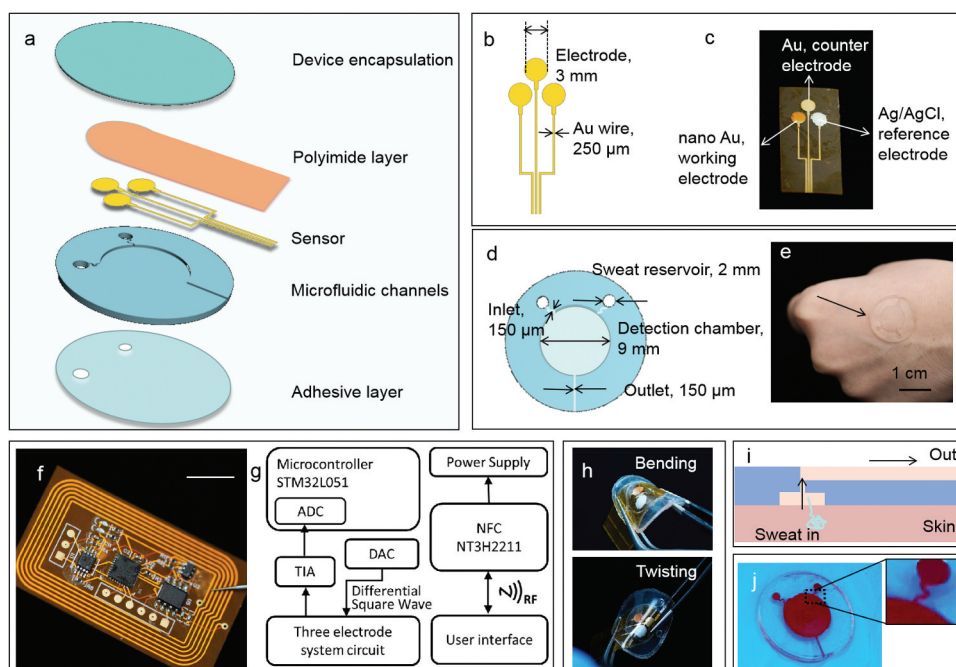


Figure 1. Overview of the flexible and wearable device for UA detection in sweat. **a** Schematic illustration of the integrated sweat sensor patch consisting of a stretchable microfluidic system and a soft UA sensor. **b** the design sketch of the three-electrode system fabricated by photolithography approach. **c** Optical imagine of the modified UA sensor. **d** the design sketch of the microfluidic system. **e** Optical imagine of the prepared microfluidic system worn on the human skin. Scale bar, 1 cm. **f** Photograph of the designed FPCB. Scale bar, 1 cm. **g** System-level block diagram describing the signal transduction, data processing, and wireless transmission. **h** Optical images of the microfluidic system integrated with the modified UA sensor under bending and twisting. **i** Schematic representation of the microfluidic system for sweat collection and guidance. **j** Photograph of its filling profile using the colored ink to clearly identify the water/air interface. The upper right image is a partially enlarged illustration.

Considering the electroactivity of UA molecules, differential pulse voltammetry (DPV) was employed to record sweat UA level on the basis of the amplitude of the oxidation peak response. DAC is programmed to release differential square pulse waves between WE and RE. Based on the DPV method, the reference current can be acquired from WE and then converted to the voltage value via transimpedance amplifier (TIA), which is read by embedded ADC in MCU. The acquired data are wirelessly transmitted to the user device over NFC for further analysis of UA concentration. It is worth mentioning that the overall dimension of the integrated device is 6.2 cm × 2.2 cm × 1.35 mm (length × width × thickness) and its weight is only 1.31 g after PDMS encapsulation. The ultra-thin and light-weighted features enable it comfortably and tightly attaches to the human skin.

Microfluidic system design and characterization

The microfluidic system was composed of two layers of PDMS, bottom channel layer and top cover layer. The bottom layer was fabricated with the assistance of a high precise 3D printed mold to form two sweat reservoirs, a reaction chamber, two inlet microfluidic channels to connect sweats reservoirs and the reaction chamber, and one outlet channel (Figure 1d). Specifically, the cylindrical sweat reservoirs were 2 mm in radius and 0.6 mm in depth. The sensing chamber was designed with the diameter of 4.5 mm and depth of 0.4 mm. All the microfluidic channels were 0.15 mm in width and 0.4 mm in depth. Therefore, the total volume capacity of the microfluidic system is approximately 10 μL . Thanks to its thin and flexible features, the designed microfluidic system can be worn on the human skin even without a medical adhesive layer (Figure 1e). What is more, it can be suitably assembled with the sensor unit (Figure S3) and can be easily bent and twisted as displayed in Figure 1h. These results reveal the outstanding potential of our system in wearable miniaturized devices.

The prepared microfluidic channel has the advantages of thinness, in-situ and efficient collection of sweat on body, and easy combination and expansion with other components. First, our microfluidic channel was fabricated via 3D printed technology, which is faster and simpler than common photolithography process. Microfluidic channel based on 3D printed technology is also low cost and unique scalability. Second, the ultra-thin and light-weighted features enable it comfortably and tightly attaches to the human skin.

Figure 1i represents the sweat collection and guidance mechanism of the microfluidic system. It is due to the capillary effect that the sweat secreted by sweat glands autonomously flows into the sensing chamber along the microfluidic channels and finally contacts with the internal detection unit to realize detection. With the help of the microfluidic system, the temporal resolution and detection accuracy of the UA sensor were greatly enhanced by continuously providing flesh sweat from the skin to the sensing chamber. In addition, all microchannels, sweat reservoirs, and detection chamber were treated with hydrophilic groups, which facilitated the delivery of sweat to the detection chamber without any extra assistance. When the resulting sweat fully filled the detection chamber, it then flowed out of the chamber and eventually gathered to the outlet. In order to simulate the sweat collection and storage functions of our microfluidic system, a fixed rate of colored ink was introduced from the inlets to the microfluidic channels. According to the related literature [38], the generation rate of sweat during active secretion is about 1.0–15 $\mu\text{L min}^{-1}$, thus 10 $\mu\text{L min}^{-1}$ was select as the fixed rate. The filling time of the microfluidic chamber was calculated as 62.1 s, suggesting the high temporal resolution of our microfluidic device. Figure 1j shows the filling profile of the microfluidic system, where almost visible areas of the sensing chamber was filled with colored ink demonstrating our microfluidic system allows for efficient sweat collection. Besides, the serpentine interconnection design (the inset in Figure 1j) of the microfluidic system follows the mechanical guideline in stretchable electronics, and therefore extremely enhances its stretchability.

Fabrication and characterization of UA sensor unit

As shown in Figure 2a, the detection principle of the UA sensor unit relies on the electroactivity of UA molecules, which can be oxidized to allantoin, accompanied by a characteristic oxidation peak. In addition, in order to meet the UA detection requirements in sweat, the UA sensor was modified with nano Au using Au electrode as matrix providing a lower detection limit. While the detection samples containing UA molecules, the oxidation peak current of UA (I_{UA}) came out at 0.25 V. The concentration of UA (C_{UA}) in the sample can be calibrated according to the fluctuation of I_{UA} . The surface morphology of nano Au was characterized by E-SEM (Figure S4). Compared with bare Au shown in Figure S5 (the inset image), nano Au formed on bare Au electrode possessed uniform burr-like structure, indicating that nano Au/Au electrode was successfully prepared.

The Au electrodes before and after modifying nano Au were evaluated in terms of the electrochemical behaviors. As can be observed in Figure 2b, the calculated surface area of nano Au electrode was 5.2 times larger than that of bare Au electrode via comparing the enclosed areas of their CV curves in 0.1 M H_2SO_4 , manifesting that the modification of nano Au effectively increased the surface area of the WE. This result may also be attributed to the elevated electron transfer rate on the electrode surface by the gold nanoparticles, thereby enhancing the electrocatalytic activity of the working electrode. The electrochemical behavior was also tested in $[Fe(CN)_6]^{3-/4-}$ probe solution. As displayed in Figure 2c, after nano Au deposition, the reversible redox peak currents significantly

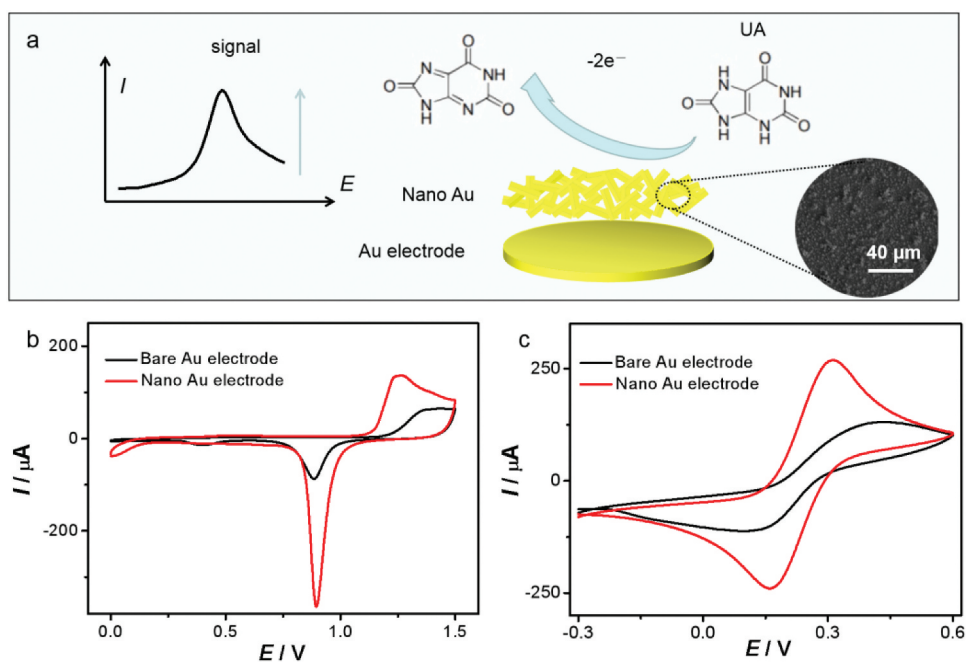


Figure 2. Electrical characterizations of the biosensor for UA determination. **a** Schematic illustration of the fabricated sensor for UA monitoring. CV curves of bare Au electrode and nano Au electrode in **b** 0.1 M H_2SO_4 and **c** 0.1 M KCl aqueous solution containing 5 mM $[Fe(CN)_6]^{3-/4-}$. The scan rate was set as 50 mV s^{-1} .

increased compared with the bare Au electrode. These results proved that nano Au electrode is superior to Au electrode due to its larger surface area and better catalytic activity.

Sensing performance for UA detection

The sensing performance of nano Au electrode-based UA sensor was assessed in terms of dynamic detection range, selectivity, long-term stability, and spike recovery. Figure 3a depicts DPV responses of the fabricated UA sensor in PBS (pH 7.2) containing UA at various concentrations. It also can be observed that the response signals of I_{UA} (~0.25 V) increased with the increase of UA concentration, owing to the fact that UA molecules were oxidized on the surface of WE. It was seen that nano Au electrode based UA sensor exhibited a wide linear relationship in the range of (5–200 μM) with the regression coefficient of 0.990 (Figure 3b). The detection limit was calculated to be 1.79 μM (S/N = 3). To evaluate reliability of the electrode preparation method, five batches of electrodes were used to detect 50 μM and 100 μM UA samples, respectively. As displayed in Figure S7, the output signals of the five batches of electrodes tended to be consistent, which proved the reliability of the electrode preparation method adopted.

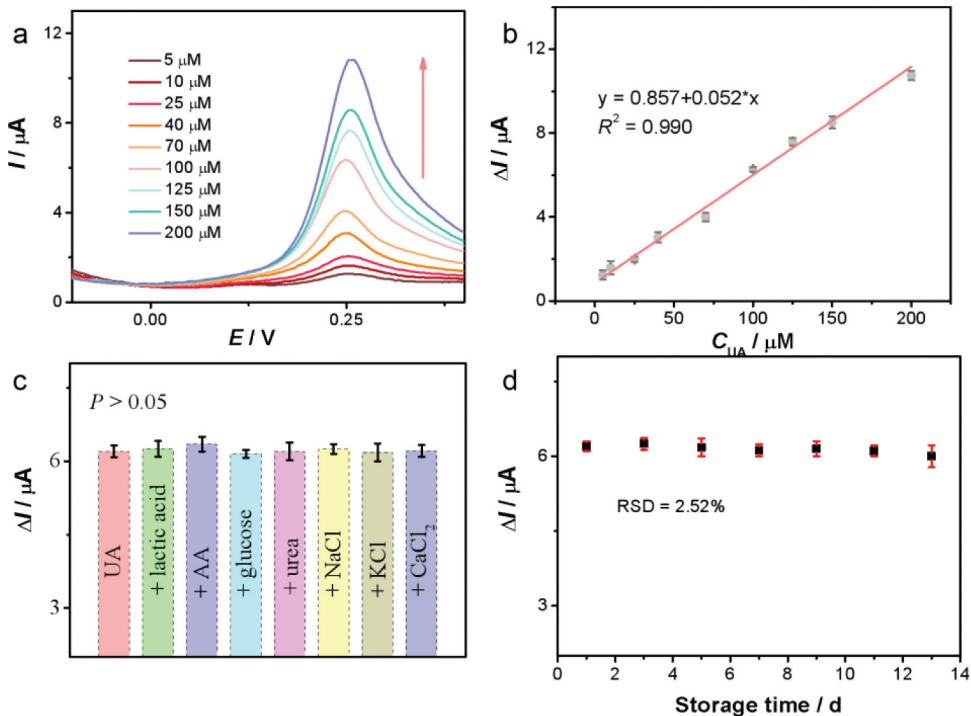


Figure 3. Sensing performance of the fabricated UA biosensor. **a** DPV responses and **b** calibration curve of the sensor in PBS (pH 7.2) containing various UA concentrations. **c** Response signals of the sensor to different electrolytes including UA alone and UA mixed with interfering substances. The concentration of UA was 100 μM and that of interferences was 500 μM . **d** Responses obtained from the prepared sensor in PBS containing 100 μM UA after storage for various time period. Error bars represent the standard deviation from three parallel tests.

The selectivity was appraised by collecting its DPV response signals at 0.25 V to diverse sweat components. In [Figure 3c](#), negligible deviations were noticed between the DPV responses at 0.25 V to pure target and the mixtures, illustrating excellent tolerance of the UA sensor to the interfering substances. Furthermore, long-term stability was also studied by testing 100 μM UA sample every day. [Figure 3d](#) depicts that there are no significant decrement in DPV signals, manifesting acceptable stability of the nano Au electrode-based UA sensor. What is more, its stability under inward and outward bending deformations was also studied as revealed in [Figure S6](#). It indicated that the signal fluctuations arising from repeated deformations were almost negligible, showing the strong mechanical stability of the fabricated sensor, further confirming its potential in wearable devices.

To appraise reliability and validity of our UA sensor unit in real-sample detection, the fabricated sensor was employed to detect UA in artificial sweat samples. As illustrated in [Table 1](#), the calculated recovery values obtained via standard addition method were in the range of 96.1–100.7%, indicating decent accuracy and feasibility of the sensor unit.

In situ sweat analysis

To realize on-body validation, the fully integrated device was mounted on human skin for in situ sweat collection and analysis. As displayed in [Figure 4a](#), it could be flexibly worn on various body parts, including arm, forehead, chest, and leg. The designed patches were applied to each of the above four body parts of one subject and the concentration of UA in perspiration were tested at 10-min intervals, where the subjects were asked to perform constant-load exercise for 30 min on a cycle ergometer ([Figure 4b-d](#)). It can be seen that the concentration of UA at different test locations were almost consistent. Meanwhile, a decreased trend in UA concentration was observed with continued perspiration as the result of profuse sweat secretion [39,40]. In addition, to further evaluate the real-time monitoring effect of our device, varied UA secretion were tested on three healthy individuals during 30-min exercise and the results were summarized in [Figure 4e](#) and [Figure S8](#). The data from commercial UA assay kit followed similar trends comparing with our wearable device as shown in [Table S1](#), demonstrating the reliability of our wearable device. These results verified that our flexible and wearable device possessed remarkable potential for in situ sweat analysis.

Table 1. Determination results of UA in artificial sweat using the fabricated sensor ($n = 3$).

Artificial sweat samples	Added (μM)	Found by the fabricated sensor (μM) ^a	Recovery (%)
1	0	–	–
	30	29.08 ± 0.12	96.9
	60	57.87 ± 0.32	96.5
2	0	–	–
	30	30.21 ± 0.44	100.7
	60	59.72 ± 0.18	99.5
3	0	–	–
	30	28.82 ± 0.38	96.1
	60	59.08 ± 0.27	98.5

^aThe data are presented as the mean \pm standard deviation.

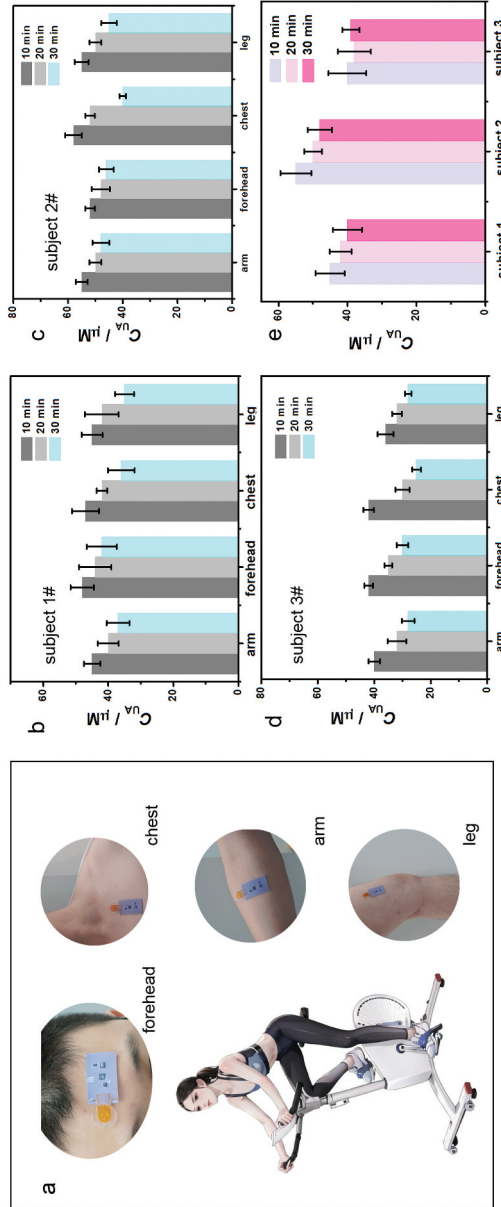


Figure 4. On-body validation of the wearable system on the skin. **a** Photographs of the wearable system mounted on different body parts of a volunteer. **b–d** Comparison of UA concentration in collected sweat at various body locations of three subjects during exercise. **e** Comparison of three subjects' UA concentration in perspiration that collected at forehead during exercise.

Conclusions

In this paper, a flexible and wearable device for in-situ sweat UA monitoring was developed via integrating a epidermal microfluidic system and a soft biosensor unit. Our wearable device enabled efficient sweat sampling, sensitive UA sensing, and wireless data processing and analysis. It also presented excellent comfortable capability by virtue of the favorable flexible and stretchable of the soft substrate. We have demonstrated the in-situ UA sensing results using our wearable device and a commercial UA assay kit toward different volunteers or various body locations during exercise. The similar fluctuation trend and high correlation obtained in our study indicated the application potential of the proposed device in wearable and intelligent sweat UA sensing. This work provides a promising design approach for the development of wearable devices. And if further combined with multiple sensing units, it is expected to be used for noninvasive monitoring of multiplexed biomarkers for applications in a variety of personalized medicine scenarios.

Materials and methods

Chemicals and apparatus

UA, lactic acid, urea, ascorbic acid (AA), glucose were supplied by Adamas Reagent Co. Ltd. (Shanghai, China). Gold acid chloride trihydrate ($\text{HAuCl}_4 \cdot 3\text{H}_2\text{O}$) was purchased from Alfa Aesar (Shanghai, China). Photoresist (PR, AZ 4620) and its related developer were purchased from the AZ Electronic Materials Co. Ltd. (Suzhou, China). Polydimethylsiloxane (PDMS, Sylgard 184 Kit) was obtained from Dow Corning Co. Ltd. (Michigan, America). Artificial sweat from Bolinda Technology Co. Ltd contains 1.2 g L^{-1} NaCl, 0.25 g L^{-1} KCl, 1.5 g L^{-1} lactic acid, 0.6 g L^{-1} urea, and 2.5 g L^{-1} acetic acid. Other reagents, such as $\text{K}_3[\text{Fe}(\text{CN})_6]$, $\text{K}_4[\text{Fe}(\text{CN})_6]$, CaCl_2 , KCl, NaCl were obtained from Sigma Aldrich Co. Ltd. (Tianjin, China) and used as received. The commercial UA assay kit was purchased from Bikese Biotechnology Co. Ltd. (Dingzhou, China).

All electrochemical measurements were conducted on an electrochemical workstation (CHI 660E, Shanghai Chenhua, China). DPV was performed from -0.2 to 0.5 V with a pulse amplitude, width and period of 50, 100, and 16.7 ms, respectively. For cyclic voltammetry (CV) test, the scan rate was set as 50 mV s^{-1} unless mentioned otherwise. And all potentials were referred to Ag/AgCl (saturated KCl solution). Surface morphology of the modified electrodes was characterized with an environmental scanning electron microscope (E-SEM, Quanta-250, American FEI Corporation). The three-electrode patch was fabricated with the help of a URE-2000 mask aligner model to operate photolithography.

Preparation of the three-electrode sensor for UA sensing

The preparation of the sensor patch was described as follows. First, the polyimide (PI) film was stucked on a glass and sequentially cleaned with deionized water (DI water), ethanol, and acetone. A layer of Cr/Au (10 nm/100 nm) was coated by E-beam. Subsequently, to obtained the three-electrode pattern, a PR layer was spin-

coated on the surface of Au membrane at 500 rpm for 10 s and 3000 rpm for 30 s, and then baked at 110°C for 5 min. The above PR/Au/Cr/PI film was exposed to ultraviolet light for 45 s with the help of custom mask and developed for 1 min in AZ 400K solution. Finally, Au and Cr were etched accordingly, followed by acetone was used to remove the residual PR. The bare three-electrode array was prepared as shown in Figure S1a.

For the working electrode (WE), electrochemical preparation of gold nanoparticles (nano Au) on Au electrode was conducted with chronoamperometry method [41]. Briefly, nano Au was electrodeposited on the surface of Au electrode in 0.5 M H₂SO₄ containing 10 mM HAuCl₄ with applied potential of 0.15 V for 100 s. For the reference electrode (RE), Ag/AgCl ink was screen-printed onto another Au electrode. The designated counter electrode (CE) was left unmodified. Finally, the fabricated sensor patches were stored at room temperature in the dark when not in use.

Fabrication of the flexible microfluidic system and the wearable device

The microfluidic system was composed of two layers of PDMS, bottom channel layer and top cover layer. Its detailed preparation process was described as follow. First, a 3D printed mold was prepared by photopolymerization of commercial photocurable polyacrylate with a high precise 3D printer. Then the mold was cleaned by acetone and isopropanol sequentially following by a heat treatment process at 80°C for 30 min to eliminate surface residual stress. After that, PDMS with the mass ratio of prepolymer and crosslinker at 10:1 was poured into the mold followed by degassing for 30 min and cure at 80°C for 2 h. The top layer of PDMS, with the mass ratio of prepolymer and crosslinker at 10:1, was fabricated by spin-coating with the spinning speed and duration of 500 rpm and 30 s, respectively. At last, the fabricated sticky PDMS capping layer was cut into pieces to bond with the UA sensing unit and the above bottom layer of microfluidic system. Then, it was connected with a designed FPCB to obtain the final flexible and wearable device.

Acknowledgments

Y.H., L.W., J.L., Y.Y., and G.Z. contributed equally to this work. This work was also sponsored by InnoHK Project on Project 2.2 – artificial intelligent (AI)-based 3D ultrasound imaging algorithm at Hong Kong Centre for Cerebro-Cardiovascular Health Engineering (COCHE), Center of Flexible Electronics Technology, and Qiantang Science and Technology Innovation Center.

Disclosure statement

No potential conflict of interest was reported by the author(s).

Ethical approval

All procedures were followed in accordance with the ethical standards of the responsible committee on human experimentation (institutional and national) and with the Helsinki Declaration of 1795, as revised in 2008 (5). The informed consent of all patients was obtained prior inclusion in the study.

References

- [1] Yamamoto Y, Yamamoto D, Takada M, et al. Efficient skin temperature sensor and stable gel-less sticky ECG sensor for a wearable flexible healthcare patch. *Adv Healthcare Mater.* 2017;6(17):1700495. doi: [10.1002/adhm.201700495](https://doi.org/10.1002/adhm.201700495)
- [2] Huang X, Liu Y, Chen K, et al. Stretchable, wireless sensors and functional substrates for epidermal characterization of sweat. *Small.* 2014;10(15):3083–3090. doi: <https://doi.org/10.1002/smll.201400483>
- [3] Kim J, Campbell AS, de Ávila BE-F, et al. Wearable biosensors for healthcare monitoring. *Nat Biotechnol.* 2019;37(4):389–406. doi: [10.1038/s41587-019-0045-y](https://doi.org/10.1038/s41587-019-0045-y)
- [4] Park S, Heo SW, Lee W, et al. Self-powered ultra-flexible electronics via nano-grating-patterned organic photovoltaics. *Nature.* 2018;561(7724):516–521. doi: <https://doi.org/10.1038/s41586-018-0536-x>
- [5] Heikenfeld J, Jajack A, Rogers J, et al. Wearable sensors: modalities, challenges, and prospects. *Lab Chip.* 2018;18(2):217–248. doi: [10.1039/C7LC00914C](https://doi.org/10.1039/C7LC00914C)
- [6] Shen H, Xue L, Ma Y, et al. Recent advances toward wearable sweat monitoring systems. *Adv Mater Technol.* 2023;8(2):2200513. doi: <https://doi.org/10.1002/admt.202200513>
- [7] Lin Y-C, Rinawati M, Chang L-Y, et al. A non-invasive wearable sweat biosensor with a flexible N-GQDs/PANI nanocomposite layer for glucose monitoring. *Sensors And Actuat B Chem.* 2023;383:133617. DOI:<https://doi.org/10.1016/j.snb.2023.133617>
- [8] Liu Y, Zhong L, Zhang S, et al. An ultrasensitive and wearable photoelectrochemical sensor for unbiased and accurate monitoring of sweat glucose. *Sensors And Actuat B Chem.* 2022;354:131204. doi: [10.1016/j.snb.2021.131204](https://doi.org/10.1016/j.snb.2021.131204)
- [9] Jeong H, Wang L, Ha T, et al. Modular and reconfigurable wireless e-tattoos for personalized sensing. *Adv Mater Technol.* 2019;4(8):1900117. doi: <https://doi.org/10.1002/admt.201900117>
- [10] Hong YJ, Lee H, Kim J, et al. Multifunctional wearable system that integrates sweat-based sensing and vital-sign monitoring to estimate pre-/post-exercise glucose levels. *Adv Funct Mater.* 2018;28(47):1805754. doi: <https://doi.org/10.1002/adfm.201805754>
- [11] Qiao L, Benziger MR, Subramony JA, et al. Advances in sweat wearables: sample extraction, real-time biosensing, and flexible platforms. *ACS Appl Mater Interfaces.* 2020;12(30):34337–34361. doi: <https://doi.org/10.1021/acsami.0c07614>
- [12] Zhao T, Zheng C, He H, et al. A self-powered biosensing electronic-skin for real-time sweat Ca²⁺ detection and wireless data transmission. *Smart Mater Struct.* 2019;28(8):085015. doi: <https://doi.org/10.1088/1361-665X/ab2624>
- [13] Nyein HYY, Gao W, Shahpar Z, et al. A wearable electrochemical platform for noninvasive simultaneous monitoring of Ca²⁺ and pH. *ACS Nano.* 2016;10(7):7216–7224. doi: <https://doi.org/10.1021/acsnano.6b04005>
- [14] Han D, Li X, Liang Z, et al. Label-free photoelectric sensor for lactic acid determination in human sweat. *Chin Chem Lett.* 2023;34(4):107722. doi: <https://doi.org/10.1016/j.ccllet.2022.08.002>
- [15] Chen CH, Lee PW, Tsao YH, et al. Utilization of self-powered electrochemical systems: metallic nanoparticle synthesis and lactate detection. *Nano Energy.* 2017;42:241–248. doi: [10.1016/j.nanoen.2017.10.064](https://doi.org/10.1016/j.nanoen.2017.10.064)
- [16] Saha T, Del Caño R, la De Paz E, et al. Access and management of sweat for non-invasive biomarker monitoring: a comprehensive review. *Small.* 2022;26:e2206064. doi: [10.1002/smll.202206064](https://doi.org/10.1002/smll.202206064)
- [17] Gai Y, Wang E, Liu M, et al. A self-powered wearable sensor for continuous wireless sweat monitoring. *Small Methods.* 2022;6(10):2200653. doi: <https://doi.org/10.1002/smt.202200653>
- [18] Cao Y, Yang Y, Qu X, et al. A self-powered triboelectric hybrid coder for human-machine interaction. *Small Methods.* 2022;6(3):2101529. doi: <https://doi.org/10.1002/smt.202101529>
- [19] Zhang Y, Guo H, Kim SB, et al. Passive sweat collection and colorimetric analysis of biomarkers relevant to kidney disorders using a soft microfluidic system. *Lab Chip.* 2019;19(9):1545. doi: <https://doi.org/10.1039/c9lc00103d>

- [20] Kim J, Jeerapan I, Imani S, et al. Noninvasive alcohol monitoring using a wearable tattoo-based iontophoretic-biosensing system. *ACS Sens.* 2016;1(8):1011. doi: <https://doi.org/10.1021/acssensors.6b00356>
- [21] Shay T, Dickey MD, Velev OD. Hydrogel-enabled osmotic pumping for microfluidics: towards wearable human-device interfaces. *Lab Chip.* 2017;17(4):710. doi: <https://doi.org/10.1039/c6lc01486k>
- [22] Ji K, Xia S, Sang X, et al. Enhanced luminol chemiluminescence with oxidase-like properties of FeOOH nanorods for the sensitive detection of uric acid. *Anal Chem.* 2023;95(6):3267–3273. doi: <https://doi.org/10.1021/acs.analchem.2c04247>
- [23] Kim I, Kim YI, Lee SW, et al. Highly permselective uric acid detection using kidney cell membrane-functionalized enzymatic biosensors. *Biosens Bioelectron.* 2021;190:113411. DOI:<https://doi.org/10.1016/j.bios.2021.113411>
- [24] Major TJ, Dalbeth N, Stahl EA, et al. An update on the genetics of hyperuricaemia and gout. *Nat Rev Rheumatol.* 2018;14(6):341–353. doi: <https://doi.org/10.1038/s41584-018-0004-x>
- [25] Terkeltaub R. Update on gout: New therapeutic strategies and options. *Nat Rev Rheumatol.* 2010;6(1):30–38. doi: <https://doi.org/10.1038/nrrheum.2009.236>
- [26] Putra BR, Nisa U, Heryanto R, et al. Selective non-enzymatic uric acid sensing in the presence of dopamine: electropolymerized poly-pyrrole modified with a reduced graphene oxide/PEDOT: PSS Composite. *Analyst.* 2022;147(23):5334–5346. doi: <https://doi.org/10.1039/D2AN01463G>
- [27] Xu Z, Song J, Liu B, et al. A conducting polymer PEDOT: PSS hydrogel based wearable sensor for accurate uric acid detection in human sweat. *Sensors And Actuat B Chem.* 2021;348:130674. DOI:<https://doi.org/10.1016/j.snb.2021.130674>
- [28] Kei A, Koutsouka F, Makri A, et al. Uric acid and cardiovascular risk: what genes can say. *Int J Clin Pract.* 2018;72(1):e13048. doi: <https://doi.org/10.1111/ijcp.13048>
- [29] Gagliardi ACM, Miname MH, Santos RD. Uric acid: a marker of increased cardiovascular risk. *Atherosclerosis.* 2009;202(1):11–17. doi: [10.1016/j.atherosclerosis.2008.05.022](https://doi.org/10.1016/j.atherosclerosis.2008.05.022)
- [30] Kohagura K, Kochi M, Miyagi T, et al. An association between uric acid levels and renal arteriopathy in chronic kidney disease: a biopsy-based study. *Hypertens Res.* 2013;36(1):43–49. doi: <https://doi.org/10.1038/hr.2012.135>
- [31] Bhole V, Choi JWJ, Woo Kim S, et al. Serum uric acid levels and the risk of type 2 diabetes: a prospective study. *Am j med.* 2010;123(10):957–961. doi: <https://doi.org/10.1016/j.amjmed.2010.03.027>
- [32] Kodama S, Saito K, Yachi Y, et al. Association between serum uric acid and development of type 2 diabetes. *Diabetes Care.* 2009;32(9):1737–1742. doi: <https://doi.org/10.2337/dc09-0288>
- [33] Makrlíková A, Opekar F, Tůma P. Pressure-assisted introduction of urine samples into a short capillary for electrophoretic separation with contactless conductivity and uv spectrometry detection. *Electrophoresis.* 2015;36:1962–1968. doi: [10.1002/elps.201400613](https://doi.org/10.1002/elps.201400613)
- [34] Cooper N, Khosravan R, Erdmann C, et al. Quantification of uric acid, xanthine and hypoxanthine in human serum by HPLC for pharmacodynamic studies. *J Chromatogr B.* 2006;837:1–10. doi: [10.1016/j.jchromb.2006.02.060](https://doi.org/10.1016/j.jchromb.2006.02.060)
- [35] Lian X, Yan B. Phosphonate MOFs composite as off-on fluorescent sensor for detecting purine metabolite uric acid and diagnosing hyperuricuria. *Inorg Chem.* 2017;56:6802–6808. doi: [10.1021/acs.inorgchem.6b03009](https://doi.org/10.1021/acs.inorgchem.6b03009)
- [36] Feng J, Li Q, Cai J, et al. Electrochemical detection mechanism of dopamine and uric acid on titanium nitride-reduced graphene oxide composite with and without ascorbic acid. *Sensors And Actuat B Chem.* 2019;298:126872. doi: [10.1016/j.snb.2019.126872](https://doi.org/10.1016/j.snb.2019.126872)
- [37] Gao W, Nyein HYY, Shahpar Z, et al. Wearable microsensor array for multiplexed heavy metal monitoring of body fluids. *ACS Sens.* 2016;1(7):866–874. doi: <https://doi.org/10.1021/acssens.6b00287>
- [38] Lin H, Tan J, Zhu J, et al. A programmable epidermal microfluidic valving system for wearable biofluid management and contextual biomarker analysis. *Nat Commun.* 2020;11(1):4405. doi: <https://doi.org/10.1038/s41467-020-18238-6>

- [39] Paul Kunnel B & Demuru S. An epidermal wearable microfluidic patch for simultaneous sampling, storage, and analysis of biofluids with counterion monitoring. *Lab Chip*. 2022;22(9):1793–1804. doi: <https://doi.org/10.1039/D2LC00183G>
- [40] Sonner Z, Wilder E, Heikenfeld J, et al. The microfluidics of the eccrine sweat gland, including biomarker partitioning, transport, and biosensing implications. *Biomicrofluidics*. 2015;9(3). doi: <https://doi.org/10.1063/1.4921039>
- [41] Yang J, Hu Y, Li Y. Molecularly imprinted polymer-decorated signal on-off ratiometric electrochemical sensor for selective and robust dopamine detection. *Biosens Bioelectron*. 2019;135:224–230. doi: [10.1016/j.bios.2019.03.054](https://doi.org/10.1016/j.bios.2019.03.054)